

Multi-scale metabolic brain connectivity construction: application to Alzheimer's disease computer-aided diagnosis

Pham Minh Tuan^{a,b,c,d}, Mouloud Adel^{*a,b,e}, Nguyen Linh Trung^d, and Eric Guedj^{a,b,c}

^aInstitut Fresnel, Aix-Marseille université, Marseille, France

^bInstitut Marseille Imaging, Marseille, France

^cCERIMED, Aix-Marseille université, Marseille, France

^dUniversity of Engineering and Technology, Vietnam National University, Hanoi, Vietnam

^eGalatasaray University, Computer Engineering Department, Istanbul, Türkiye

* Corresponding author email address: mouloud.adel@univ-amu.fr, phone: +33 6 72 53 01 85

Abstract

This study introduces a novel method for constructing multi-scale individual brain networks from static Fluorodeoxyglucose Positron Emission Tomography (FDG-PET) images, with a primary focus on diagnosing Alzheimer's Disease (AD). Using Schaefer atlases, we partition the brain image into distinct regions, treating them as nodes in the graph. Subsequently, the Kernel Density Estimation (KDE) and Wasserstein Distance (WD) algorithms are used to estimate similarities between brain regions, forming graph connections. Addressing limitations inherent in fixed KDE settings, we propose employing several methods: the interquartile range, Sturges', and Freedman-Diaconis rules, to optimize KDE settings. WD, renowned for its ability to capture both probability and spatial differences, is used to enhance the comparison of similarities among graph nodes. The effectiveness of our method is validated using the ADNI dataset. Connectivity analysis across diagnostic groups—Cognitive Normal (CN), Mild Cognitive Impairment (MCI), and AD—reveals disruptions in information transmission within the FDG-PET based brain network of MCI and AD subjects, compared to CN. Our findings support the effectiveness of KDE and WD in constructing multi-scale individual brain networks from FDGPET images. This method shows promise for applications in other brain disorders, enabling personalized diagnosis.

Keywords: Fluorodeoxyglucose Positron Emission Tomography, FDG-PET; Individual brain network; Kernel Density Estimation; Wasserstein Distance; Alzheimer's Disease.

1. Introduction

Alzheimer's Disease (AD) is a major type of neurodegenerative brain disease prevalent among the elderly population. In 2018, an estimated 50 million people worldwide were living with dementia, and this number is projected to reach 152 million by 2050 (Patterson, 2018). Timely detection of AD plays a vital role in ensuring appropriate patient care in the context of approval of emerging therapeutics acting on disease course. Biomarkers, including Fluorodeoxyglucose Positron Emission Tomography (FDG-PET) images, have demonstrated effectiveness in early AD diagnosis (Alberdi et al., 2016, Guedj et al., 2022). In recent years, FDG-PET based brain network analysis has proven to be an effective tool for understanding brain functions, its alterations under various conditions of AD, as well as for better diagnosing AD (Huang et al., 2018, Yao et al., 2017, Wang et al., 2020). Even though, the early studies on FDG-PET-based networks have primarily focused on group-based analyses, which may result in losing specific information within an individual brain (Wang et al., 2020). Meanwhile, recent studies have

highlighted the significance of investigating individual-level brain networks as a promising tool offering valuable insights into personalized brain profiles and their implications for understanding brain disorders (Wang et al., 2020, Huang et al. 2020, Li et al., 2023).

One of the main challenges in constructing individual brain networks from static FDG-PET images, compared to other neuroimaging modalities, such as functional Magnetic Resonance Imaging, is that static FDG-PET only captures brain metabolism at a specific point in time, making it difficult to study the brain network at the individual level. To address this problem, a few methods based on Kernel Density Estimation (KDE) have been used (Wang et al., 2020, Li et al., 2023). Although these studies have produced interesting results, there is a limitation in the way KDE is applied.

Notably, KDE settings have a significant effect on individual network analysis. In previous studies (Wang et al., 2020, Li et al., 2023), when using KDE, after using observed data to estimate the Probability Density Function (PDF) for a brain region, they typically estimate KDE on a

fixed range of values with the same number of sample points for all brain regions. These values are then used to compare the similarity between two PDFs of two brain regions. This approach generally exhibits several limitations. Firstly, there are significant differences in terms of sizes for various brain regions. Secondly, range values for the same brain regions may vary between subjects belonging to different groups (such as healthy control and patient groups). Therefore, using fixed settings for range values and sampling points may lead to the loss of information or over/underestimation. Thirdly, choosing the appropriate fixed settings also requires experiments, which is a time-consuming process. Fourthly, when working with brain networks at multiple scales, the need to select appropriate settings to well represent PDFs is crucial and unavoidable. To overcome these limitations, in this study, we propose a new approach for building FDG-PET-based individual graph, in which, KDE estimation is adapted in terms of range values and sampling points based on observations from the data. We refer to this as data-driven KDE estimation. Additionally, to capture both probability differences and variations in range values when comparing two PDFs, we use Wasserstein distance (WD) as a similarity metric. With this approach, we expect that our approach is more suitable for studying individual brain networks at different scales.

In short, in this study, we proposed several improvements in the way of constructing individual brain networks using KDE estimation from static FDG-PET images and their application in AD analysis. More specifically, our contributions can be summarized as follows:

- We select more optimal settings for KDE: estimating KDE at an adapted value range and number of sampling points using the concept of Interquartile Range (IQR), Sturge’s, and Freedman-Diaconis rules.
- We apply Wasserstein distance to compare the similarity between two KDEs: building brain networks at multiple scales using Schaefer atlases.
- We validate the effectiveness of the proposed method on the ADNI dataset: performing connectivity analysis across various stages of AD and comparing the sensitivity of the proposed method with a baseline method.

With this study, our primary objective is to validate the effectiveness of adapted KDE settings, and Wasserstein distance in constructing individual brain networks at multiple scales.

2. Materials and Methods

2.1 Dataset

Data used in the experiment is 18F-FDG PET images downloaded from the Alzheimer’s Disease Neuroimaging Initiative (ADNI) database. In the ADNI dataset, participants can take several scans at different time points, the first time of scan refers to a baseline scan. Time points after baseline are considered as follow-up time. Data is selected based on following criteria:

- Cognitive Normal (CN) - subjects diagnosed as cognitive control at the baseline and do not change over time.
- stable Mild Cognitive Impairment (sMCI) – subjects diagnosed as MCI at the baseline and did not convert to AD in the follow-up period at least 24 months.
- progressive MCI (pMCI) - subjects diagnosed as MCI at the baseline and progressed to AD in the available scan time.
- Alzheimer’s Disease (AD) - subjects diagnosed as Alzheimer’s disease at the baseline and do not change within the follow-up time.

The data is then pre-processed by the following steps: spatially normalized to a standard template, smoothed, and intensity normalization. More details about these steps can be found in (Tuan et al., 2023). The demographic and clinical information of subjects is provided in Table I, in which MMSE stands for the Mini Mental State Examination (Mitchell, 2009).

2.2 Methods

The flowchart of the proposed method is depicted in Fig. 1. To construct an individual graph from a single FDG-PET image, we need to determine nodes and connections. Here, we use predefined atlases, Schaefer atlases (Schaefer et al., 2018), to separate the brain into regions of interest (ROI) and treat each region as a node. The connections between nodes are computed using KDE to estimate the PDF of voxel values in each region, and Wasserstein distance to assess PDF similarity. More details about these steps are provided in the following sections.

a) Node Representations (KDE-based phase):

In this study, we use Schaefer atlases at multiple scales (100, 200, 300, and 500 regions) to define the nodes. Specifically, the Schaefer atlas is used to segment the brain image into ROIs, treated as nodes. We then extract voxel intensity values within each ROI and use them to estimate the PDF using the KDE method.

KDE method is a non-parametric technique used to estimate the PDF of a random variable based on a set of observed data points (Weglarczyk, 2018). The KDE estimation process involves placing a kernel on each data point and then summing up these kernels to obtain the density estimate. In our study, KDE is applied to each brain region in the FDG-PET image to estimate the underlying distribution of glucose metabolism levels within that region. Following that, we use KDE to estimate values of PDF at specific points, employing these points to compare the similarity between PDFs of two ROIs.

However, instead of using KDE at a specific value range and a fixed number of points as in previous studies (Wang et

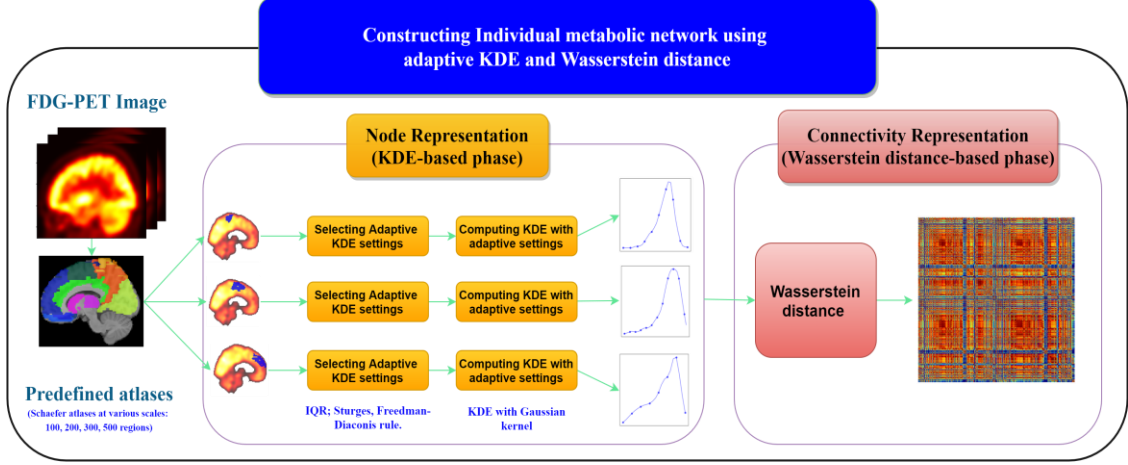


Fig. 1. Workflow for constructing an individual graph from a static FDG-PET image.

Table I. Demographic and Clinical information of subjects

Characteristic	CN	sMCI	pMCI	AD
Number of subjects	242	360	209	237
Female/Male	122/120	153/207	87/122	97/140
Age (Mean \pm std.)	73.66 \pm 5.66	71.73 \pm 7.66	73.89 \pm 6.88	75.00 \pm 7.91
MMSE (Mean \pm std.)	29.03 \pm 1.20	28.20 \pm 1.59	27.13 \pm 1.71	23.19 \pm 2.12

al., 2020, Li et al., 2023), we use the IQR to select optimal range values and apply Sturges’ and Freedman-Diaconis rules to determine the optimal number of sample points. More details about these steps are described below.

Data range selection using IQR: The optimal range value for each region is estimated using concept of 1.5 IQR. The IQR, calculated as the difference between the third quartile (Q_3) and the first quartile (Q_1), captures the middle 50% of the data. To identify potential outliers and establish data limits, a multiplier of 1.5 times the IQR is employed, striking a balance between outlier sensitivity and preservation of valuable data. Lower and upper limits are determined by subtracting and adding 1.5 times the IQR to Q_1 and Q_3 , respectively:

$$\text{LowerLimit} = Q_1 - 1.5 \times \text{IQR},$$

$$\text{UpperLimit} = Q_3 + 1.5 \times \text{IQR}.$$

This method, widely accepted in data analysis, proves particularly useful for creating box-and-whisker plots and conducting preliminary outlier detection (Hubert and Vandervieren, 2008).

Selecting number of sampling points for PDF: To compare two PDF functions, the easiest method is to evaluate them at a set of sampling bins. Selecting the appropriate number of bins is crucial. In this study, we combine Sturges’ rule and the Freedman-Diaconis rule to determine the optimal one.

Sturges Rule : is a simple and widely used formula for estimating the number of bins (k) in a histogram (Scott, 2007). It is based on the assumption of a normal distribution and is defined as: $k_{\text{Sturges}} = 1 + \log_2(n)$, where n is the number of data points in the dataset. Sturges’ rule tends to produce

histograms with a moderate number of bins, suitable for visualizing general data distributions.

Freedman-Diaconis Rule : provides a more robust approach to bin estimation, taking into account the data’s spread and potential outliers (Birgé and Rozenholc, 2006). It is defined as: $k_{\text{FD}} = \frac{2 \times \text{IQR}(x)}{n^{-1/3}}$, where $\text{IQR}(x)$ is the interquartile range. In our case, for each ROI, x and n correspond to all voxels belonging to the region and its total number of voxels, respectively. The Freedman-Diaconis rule yields a larger number of bins when the data exhibits greater variability or the presence of outliers, ensuring a more detailed representation.

We then select the maximum of these two values as the optimal number of points: $k_{\text{KDE}} = \max(k_{\text{Sturges}}, k_{\text{FD}})$. This approach allows us to adapt the binning strategy to the characteristics of the dataset, ensuring that our sampling points effectively capture the underlying data distribution while avoiding under-simplification or over-complication.

b) **Connectivity Representations (WD-based phase):**

Once KDE, with the proposed improvements, is applied to the FDGPET data for each brain region, the Wasserstein distance (Panaretos and Zemel, 2019) is utilized to compute the dissimilarity between the metabolic activity patterns of all possible pairs of brain regions. The Wasserstein distance, denoted as $WD(P, Q)$, quantifies the distance between two PDFs P and Q :

$$WD(P, Q) = \min_{\gamma \in \Gamma(P, Q)} \sum_{i, j} \gamma_{ij} \cdot d(x_i, y_j)$$

Here, γ represents a transportation plan specifying mass movement from x_i in P to y_j in Q . The transportation plan γ

belongs to the set $\Gamma(P, Q)$, which consists of all possible valid transportation plans. γ_{ij} represents the amount of mass to be transported from x_i to y_j according to the transportation plan γ . $d(x_i, y_j)$ represents the distance or dissimilarity between the points x_i and y_j in the PDFs. To compute the Wasserstein distance, we identify the optimal transportation plan γ minimizing total cost, further details can be found in (Ramdas et. Al., 2017). One of the advantages of WD for comparing the similarity between two PDFs is its consideration of both probability differences and variations in the range of values.

Based on the WD between two ROIs, the connection between two nodes is computed as $c_{WD(P,Q)} = e^{-WD(P,Q)}$. For each FDG-PET image, applying this process for any pair of ROIs yields a similarity matrix that quantifies the connection between brain regions. This matrix forms the basis for further network analysis.

c) Connectivity Analysis:

To evaluate the effectiveness of our proposed method, we analyze connectivity matrices from two different perspectives:

- *Visualization:* We plot connectivity matrices to determine whether it is possible to capture differences between various stages of AD.
- *Classification:* We use connectivity matrices as features for training Support Vector Machine (SVM) classifiers on various AD classification tasks. To evaluate the effectiveness, we compare the performance between our proposed method and a baseline method. Specifically, we use Kullback-Leibler Similarity (KLS) Wang et al., 2020) with fixed settings of KDE as the comparison method.

For the classification task, we implement a 5-fold cross-validation. To mitigate biases, we conduct experiments 100 times and report the averaged results.

3. Results and Discussion

3.1 Results

a) Visualizing the Connectivity Matrices:

The connectivity matrices show the differences between various stages of AD: Fig. 2 compares the average connectivity matrices using the proposed method at different stages of AD (from left to right: CN, sMCI, pMCI, and AD, respectively) and at different scales of Schaefer atlases (from top to bottom: 100, 200, 300, and 500 regions, respectively). In the first row (networks with 100 regions), a decreasing trend in connectivity measures is observed as the disease progresses. When comparing the CN group to other groups, subtle differences exist between CN and sMCI, while significant differences are apparent between CN and pMCI, as well as AD. The most notable differences are found in regions belonging to the Default Mode Network (DMN) of the Schaefer atlas (Schaefer et al., 2018). Similar trends are observed in the other rows of Fig. 2. When comparing different rows, it becomes evident that, while similar trends persist, the higher scale (e.g., Schaefer 500 regions) provides

more precise information about the regions where the changes occur. The above observations suggest that the proposed method demonstrates the capability to capture differences between various stages of AD, and indicating the effectiveness of the adapted settings for KDEs.

The decreasing trend in the number of connections between various stages of AD: Fig. 3 depicts the relationship between threshold values and the proportion of strongest connections. We observe that, at the same threshold value, the number of connections in the CN group is higher compared to pMCI and AD, while very similar to sMCI. This observation holds true across all network scales. These findings imply that, at the same threshold of connectivity values, the network of AD patients has fewer connections compared to that of CN subjects. In other words, this indicates diminished effectiveness in information transmission between nodes in the brain networks of the disease groups.

The decreasing trend is also observed at the subject level: Fig. 4 provides a more detailed comparison based on a subject connectivity matrix. Specifically, the figure compares connectivity matrices for a randomly selected subject from each group—CN, sMCI, pMCI, and AD—across various network scales. It is easy to observe that there is a decrease in connectivity value when comparing CN subjects with pMCI and AD subjects, and between pMCI and AD subjects. Additionally, higher network scales seem to provide more precise information about regions where changes occur. These observations suggest that our method also has the capability to capture changes at the individual level.

The above observations highlight a consistent decline in connectivity values across different stages and scales of AD networks. It indicates a significant loss of connectivity within the AD groups, implying reduced efficiency in information transmission within the brain networks. These findings collectively provide evidence supporting the efficacy of our proposed method in constructing networks at various scales and detecting changes within networks at both group and individual levels.

b) Performance on Classification Tasks:

The importance of multiple scale analysis: Tables II, III and Fig. 5 present a comparative analysis of SVM classifier performance using connectivity matrices obtained through different methods, including Wasserstein Distance with fixed and adapted KDE settings (referred to as WD and WA, respectively), alongside a baseline method (KLS) that utilizes fixed KDE settings. These analyses are conducted across diverse classification tasks (AD and MCI classification) and scales of the Schaefer atlas (100, 200, 300, 500 regions). Overall, we consistently observe that increasing scales (number of regions) contribute to a slight improvement in performance. This observation can be seen across different methods, as well as various classification tasks. Specifically, using the Schaefer atlas with 500 regions

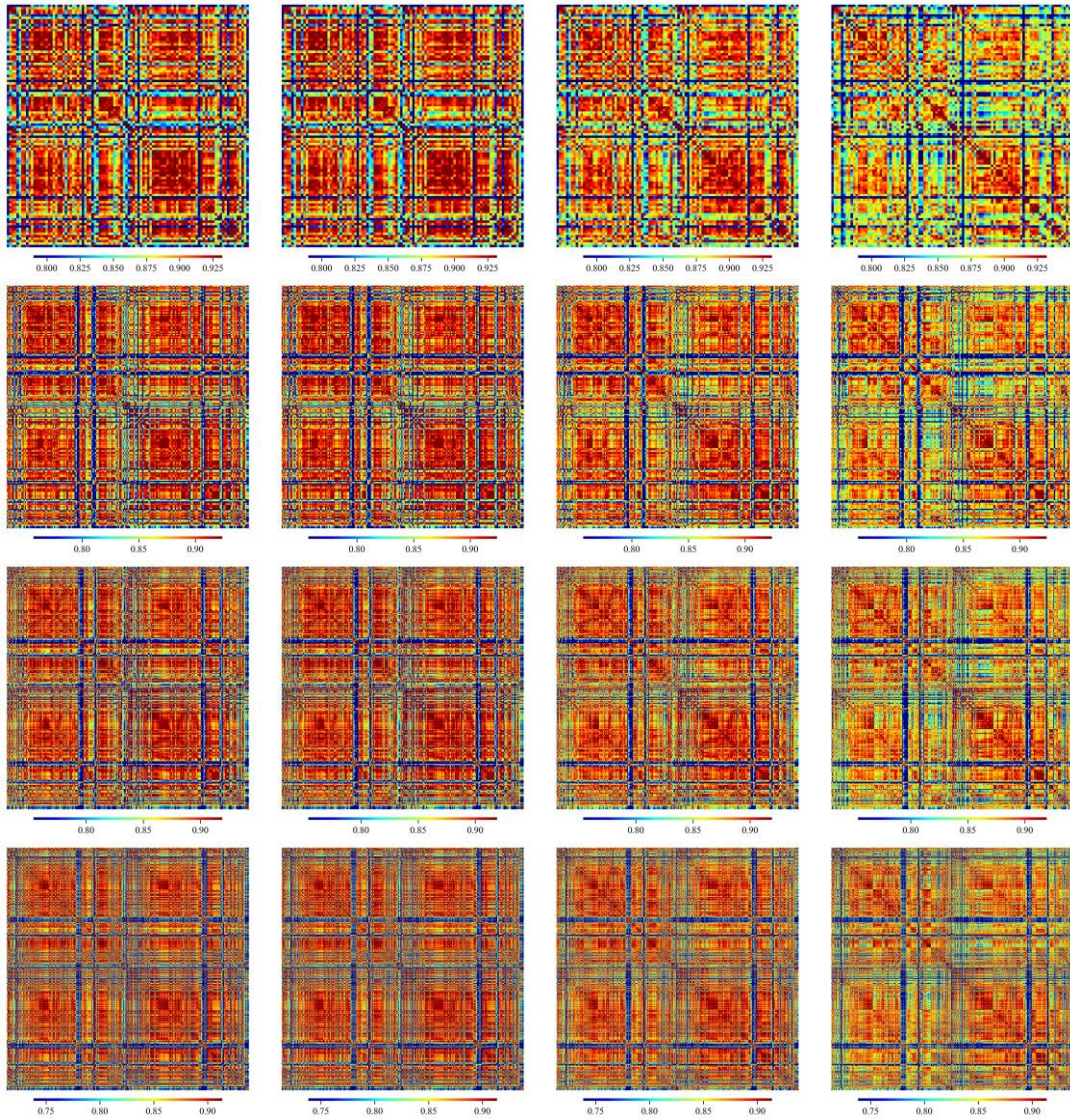


Fig. 2. The average similarity matrices between various stages of AD, including (from left to right) CN, sMCI, pMCI, and AD, are calculated using Schaefer atlases with (from top to bottom) 100, 200, 300, and 500 regions.

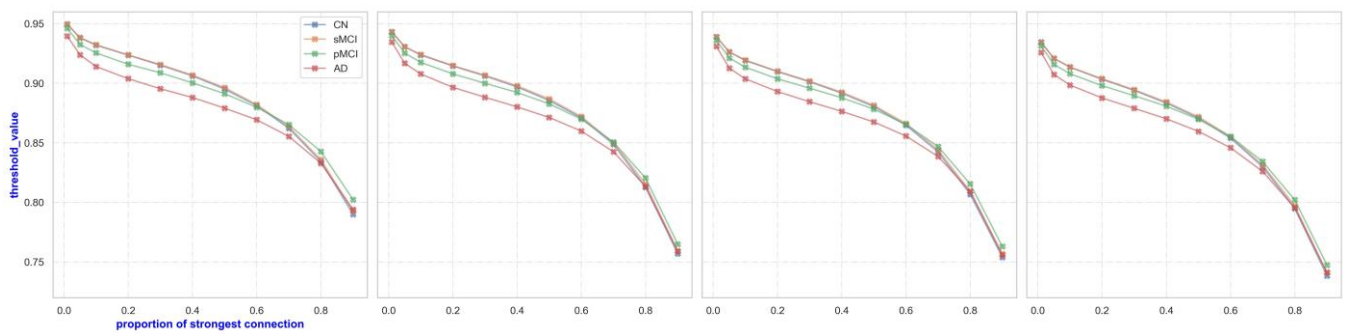


Fig. 3. Relationship between threshold Values and strongest Connections Proportion across various stage of AD, computed based on average similarity matrices.

increases performance by approximately 1-4 percent across all metrics and tasks when compared with using the Schaefer atlas with 100 regions. This observation emphasizes the advantage of exploring higher scales. However, certain instances reveal competitive performance at lower scales, such as KLS with 200 regions in the MCI task. This observation indicates that performance may not always linearly correlate with the number of regions used. All of those observations provide evidence for the advantages of studying multiple scales, emphasizing the importance of considering different scales in the analysis.

Table II. Performance on CN vs. AD classification task

	ACC	SEN	SPE	AUC
KLS + Schaefer (100)	85.44	84.54	86.33	92.79
KLS + Schaefer (200)	87.83	86.27	89.36	93.26
KLS + Schaefer (300)	87.25	85.46	89.01	93.25
KLS + Schaefer (500)	89.03	87.36	90.67	94.43
WD + Schaefer (100)	90.08	88.22	91.90	95.34
WD + Schaefer (200)	88.83	88.47	89.17	95.21
WD + Schaefer (300)	89.48	89.30	89.65	95.85
WD + Schaefer (500)	91.54	90.75	92.31	96.72
WA + Schaefer (100)	90.07	88.23	91.88	95.33
WA + Schaefer (200)	88.95	88.49	89.38	95.27
WA + Schaefer (300)	89.67	89.43	89.90	95.94
WA + Schaefer (500)	91.61	90.84	92.35	96.83

KLS and WD use fixed KDE settings for different scales of the Schaefer atlases, while WA uses adaptive KDE settings selected by IQR, Sturges', and Freedman-Diaconis rules.

Table III. Performance on sMCI vs. pMCI classification task

	ACC	SEN	SPE	AUC
KLS + Schaefer (100)	71.21	57.44	79.19	75.13
KLS + Schaefer (200)	72.43	58.23	80.67	76.49
KLS + Schaefer (300)	72.49	56.60	81.71	75.84
KLS + Schaefer (500)	71.28	55.78	80.28	75.26
WD + Schaefer (100)	70.26	57.51	77.67	75.14
WD + Schaefer (200)	69.87	58.79	76.31	74.84
WD + Schaefer (300)	69.89	58.00	76.79	75.06
WD + Schaefer (500)	72.73	60.15	80.03	76.89
WA + Schaefer (100)	70.59	57.60	78.12	75.32
WA + Schaefer (200)	69.81	58.67	76.28	74.73
WA + Schaefer (300)	69.71	57.86	76.60	74.92
WA + Schaefer (500)	72.73	60.12	80.04	76.68

The effectiveness of Wasserstein Distance: When comparing methods with fixed KDE settings (KLS vs. WD) in Fig. 5, WD generally outperforms KLS, especially in AD classification. However, in MCI classification, KLS shows slightly better performance at lower scales, while WD demonstrates comparable or superior performance at higher

scales, suggesting its competitiveness. This observation can be attributed to WD's similar or superior capability in detecting group differences compared to KLS when using the same KDE settings.

The effectiveness of adapted KDE settings: Comparing adapted KDE settings to fixed settings (WA vs. KLS, WD), WA's performance is either better or closely comparable to WD. Notably, with 500 regions, WA outperforms KLS and slightly improves upon WD, especially in AD classification. This highlights the comparative advantage of adaptive settings over fixed KDE settings and emphasizes the suitability of adaptive KDE settings and Wasserstein distance for comparing group differences.

Our findings collectively underscore the advantages of studying higher scales, emphasizing the importance of exploring multiple scales. Additionally, all observations provide evidence for the benefits of employing adaptive KDE settings and Wasserstein distance in computing similarity matrices. This implies that by utilizing our proposed method (WA), we can save time typically spent on experiments with KDE settings, while also expecting very comparable performance. This streamlines the process of constructing similarity matrices and enhances efficiency.

3.2 Discussion

Align with prior studies: Both the pMCI and AD groups exhibited lower connectivity values compared to the CN group. This reduced connectivity, particularly pronounced in the DMN, suggests that, at the same threshold of connectivity values, the network of AD patients has fewer connections compared to that of CN subjects. In other words, this indicates diminished effectiveness in information transmission between nodes in the brain networks of the disease groups. This finding is consistent with previous studies (Farahani et al., 2019), (Zhong et al., 2014) that showed a significant reduction in the number of connections in DMN during the later phase of AD. Furthermore, decreasing trends in connectivity matrices between various stages of AD were also observed in previous studies with both group-based and individual brain networks (Huang et al., 2017), (Huang et al., 2020).

Effectiveness of the Proposed Method: Our proposed method consistently demonstrates comparable or superior performance to the baseline when employing connectivity matrices as features for classification tasks. This, combined with its ability to showcase distinct visual patterns across various stages of AD, suggests that our method is effective in capturing distinctions among these stages, thereby enhancing diagnostic capabilities. The superior performance of our proposed method can be attributed to our strategy of selecting adapted settings for KDE and combining it with the WD, which is well-known for capturing probability differences. Consequently, our method becomes more adaptive in building metabolic brain networks.

The need for multi-scale analysis: Fig. 6 compares the performance of the proposed methods and the baseline method across various scales. Our observations indicate that, for AD classification, increasing the scale generally

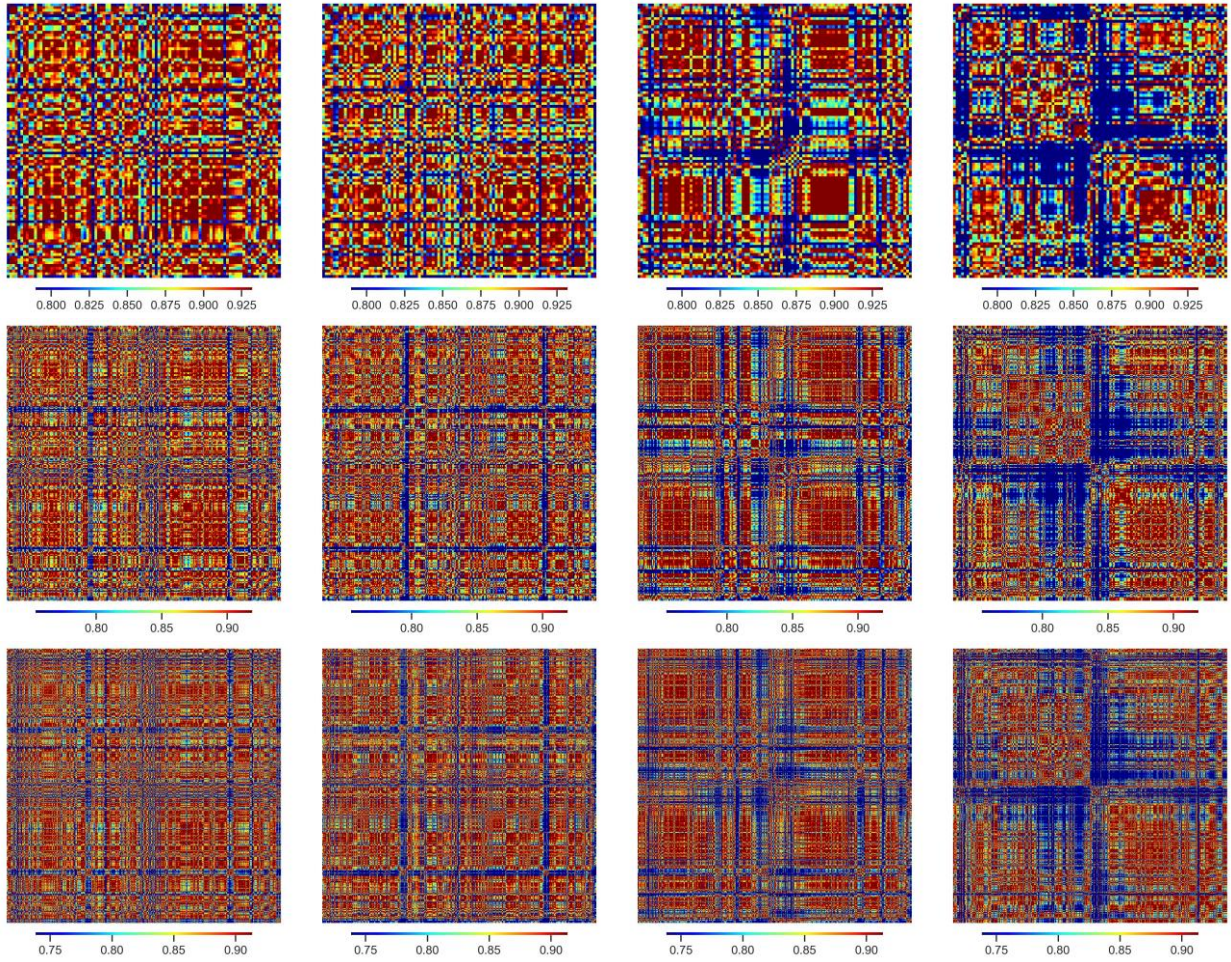


Fig. 4. The similarity matrices for random selected subject in each group of data, including (from left to right) CN, sMCI, pMCI, and AD, are calculated using Schaefer atlases with (from top to bottom) 100, 300 and 500 regions.

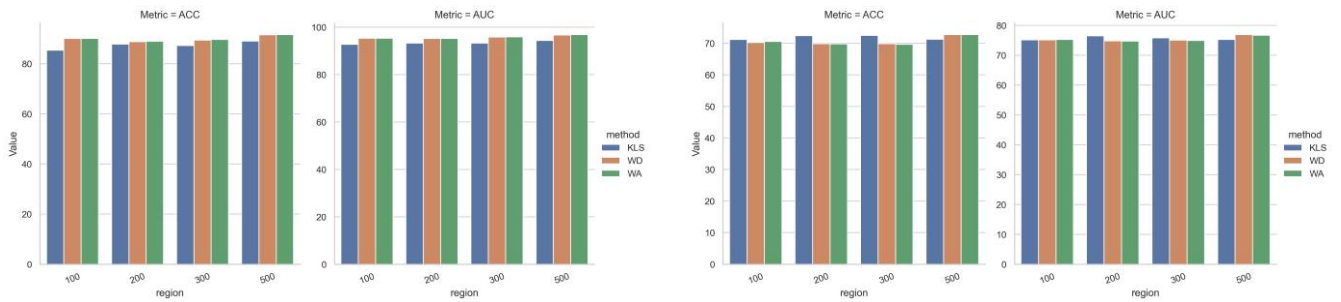


Fig. 5. Comparison of performance between proposed methods (WD, WA) and the baseline method (KLS) on the AD (left) and MCI (right) classification task.

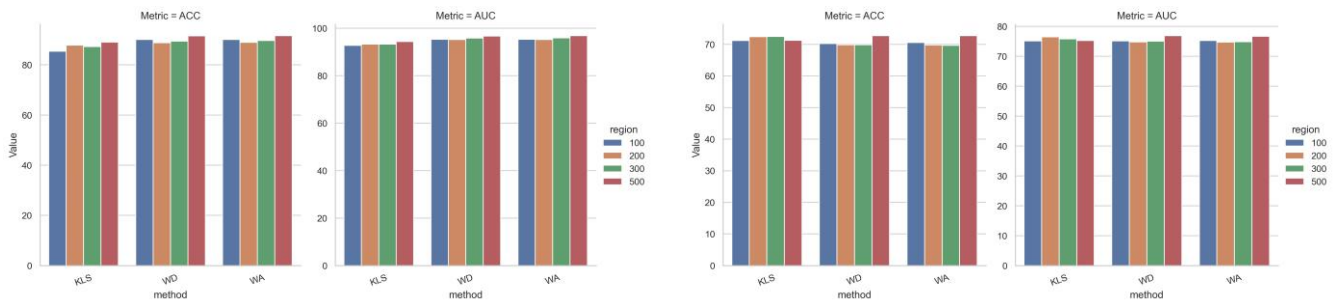


Fig. 6. Comparison of the dependence of performance on network scales for the AD (left) and MCI (right) classification tasks.

enhances performance. However, for the MCI classification task, this trend is not consistently observed. These variations across different scales and classification tasks suggest that each scale has its own capability to capture information. Therefore, the choice of scale is critical and depends on multiple factors, including the specific method and task. This underscores the importance of multi-scale analysis and suggests that integrating insights from different scales can potentially lead to overall performance improvement.

Future work: Further experiments on other brain diseases and datasets are necessary to validate the effectiveness of the proposed method. Moreover, in this study, we assumed that the PDF follows a Gaussian distribution. However, this assumption may not hold true in reality. Therefore, conducting additional experiments with different PDF shapes and investigating the relationship between adaptive KDE settings and the dataset characteristics is crucial. Additionally, although our analysis is preliminary, future research could delve into graph metric analysis (Sporns, 2018) or explore the application of graph neural networks (Wu et al., 2020) to enhance diagnostic performance.

4. Conclusion

In this study, we introduced a novel method utilizing KDE and WD to construct multi-scale individual brain networks from FDG-PET images. Instead of relying on fixed KDE settings, we selected optimal settings using IQR, Sturges', and Freedman-Diaconis rules. Our approach revealed disruptions in information transmission within brain networks across various AD stages and supports the effectiveness of KDE and Wasserstein in constructing multi-scale brain networks. This method shows promise for applications in diagnosing other brain disorders, enabling personalized diagnosis.

Acknowledgments

Pham Minh Tuan was supported by A*MIDEX program (AMX-19-IET-002) of Aix-Marseille University for his PhD scholarship. The research of Nguyen Linh Trung and Pham Minh Tuan was funded by Vietnam National Foundation for Science and Technology Development (NAFOSTED) under grant number 102.04-2021.55.

Data used in preparation of this article were obtained from the Alzheimer's Disease Neuroimaging Initiative (ADNI) database (adni.loni.usc.edu). As such, the investigators within the ADNI contributed to the design and implementation of ADNI and/or provided data but did not participate in analysis or writing of this report. A complete listing of ADNI investigators can be found at: http://adni.loni.usc.edu/wpcontent/uploads/how_to_apply/ADNI_Acknowledgement_List.pdf

References

C. Patterson, C. (2018). World Alzheimer Report 2018: The State of the Art of Dementia Research. Alzheimer's Disease International, London.

Alberdi, A, Aztiria, A, Basarab, A, (2016). On the early diagnosis of Alzheimers Disease from multimodal signals: A survey. *Artificial Intelligence in Medicine*, vol. 71, pp. 1-29, 7.

Guedj, E et al, (2022). EANM procedure guidelines for brain PET imaging using [18 F] FDG, version 3. *European Journal of Nuclear Medicine and Molecular Imaging*, pp. 1-20, 2022.

Huang, SY, Hsu JL, Lin KJ, Liu HL, Wey SP, Hsiao IT, (2018). Characteristic patterns of inter- and intra-hemispheric metabolic connectivity in patients with stable and progressive mild cognitive impairment and Alzheimer's disease. *Scientific Reports*, vol. 8.

Yao, Z, Hu, B, Chen, X, Xie, Y, Gutknecht, J, D. Majoe, D, (2017). Learning Metabolic Brain Networks in MCI and AD by Robustness and Leave-One-Out Analysis: An FDG-PET Study. *American Journal of Alzheimer's Disease & Other Dementias*, vol. 33, p. 42–54, 9.

Wang, M, Jiang, J, Yan, Z, Alberts, I, Ge, J, Zhang, H, Zuo, C, Yu, J, Rominger, A, Shi, F, (2020). Individual brain metabolic connectome indicator based on Kullback-Leibler Divergence Similarity Estimation predicts progression from mild cognitive impairment to Alzheimer's dementia. *European Journal of Nuclear Medicine and Molecular Imaging*, vol. 47, p. 2753–2764, 4.

Huang, SY, Hsu, JL, Lin, KJ, Hsiao, IT, (2020). A Novel Individual Metabolic Brain Network for 18F-FDG PET Imaging. *Frontiers in Neuroscience*, vol. 14, 5.

Li, W, Tang, Y, Peng, L, Wang, Z, Hu, S, Gao, X, (2023). The reconfiguration pattern of individual brain metabolic connectome for Parkinson's disease identification. *MedComm*, vol.4, no.4, p.e305, 2023, doi: 10.1002/mco2.305.

Tuan, PM, Trung, NL, Adel, M, Guedj, E, (2023). Auto Encoder-based Feature Ranking for Predicting Mild Cognitive Impairment Conversion using FDG-PET Images. *2023 IEEE Statistical Signal Processing Workshop (SSP)*, Hanoi, Vietnam: IEEE, pp. 720–724. doi: 10.1109/SSP53291.2023.10208072.

Mitchell, AJ, (2009). A meta-analysis of the accuracy of the minimal state examination in the detection of dementia and mild cognitive impairment. *Journal of Psychiatric Research*, vol. 43, no. 4, pp. 411431.

Schaefer A et al. (2018). Local-Global Parcellation of the Human Cerebral Cortex from Intrinsic Functional Connectivity MRI. *Cerebral Cortex*, vol. 28, no. 9, pp. 3095–3114, doi: 10.1093/cercor/bhx179.

Weglarczyk, S, (2018). Kernel density estimation and its application," *ITM Web of Conferences*, vol. 23, p. 00037.

Hubert M, Vandervieren, E, (2008). An adjusted boxplot for skewed distributions. *Computational Statistics & Data Analysis*, vol. 52, no. 12, pp. 5186–5201, doi: 10.1016/j.csda.2007.11.008.

Scott, DW, (2009). Sturges' rule. *WIREs Computational Stats*, vol. 1, no. 3, pp. 303–306, doi: 10.1002/wics.35.

Birgé, L, Rozenholc, Y, (2006). How many bins should be put in a regular histogram. *ESAIM: PS*, vol. 10, pp. 24–45, doi: 10.1051/ps:2006001.

Panaretos VM, Zemel, Y, (2019). Statistical specs of Wasserstein Distances. *Annu. Rev. Stat. Appl.*, vol. 6, no. 1, pp. 405–431, doi: 10.1146/annurev-statistics- 30718-104938.

Ramdas, A, N. Trillos, N, M. Cutu M, (2017). On Wasserstein Two-Sample Testing and Related Families of Nonparametric Tests. *Entropy*, vol. 19, no. 2, p. 47, doi: 10.3390/e19020047.

- Farahani, FV, Karwowski, W, Ligthall, NR, (2019). Application of Graph Theory for Identifying Connectivity Patterns in Human Brain Networks: A Systematic Review. *Front. Neurosci.*, vol. 13, p. 585, doi: 0.3389/fnins.2019.00585.
- Zhong Y et al., (2014). Altered effective connectivity patterns of the default mode network in Alzheimer's disease: An fMRI study. *Neuroscience Letters*, vol. 578, pp. 171–175, Aug. 2014, doi: 10.1016/j.neulet.2014.06.043.
- Sporns, O, (2018). Graph theory methods: applications in brain networks. *Dialogues in Clinical Neuroscience*, vol. 20, no. 2, pp. 111-121.
- Wu Z et al., (2020). A comprehensive survey on graph neural networks. *IEEE Transactions on Neural Networks and Learning Systems*, vol. 32, no. 1, pp. 4-24.